INSTITUTE OF PHYSICS PUBLISHING SMART MATERIALS AND STRUCTURES
Smart Mater. Struct. **14** (2005) 1343–1352 doi:10.1088/0964-1726/14/6/026

Theoretical modeling, experiments and optimization of piezoelectric multimorph

Seung-Yop Lee[1], **Byeongsik Ko**[2,3] **and Woosung Yang**[1]

[1] Department of Mechanical Engineering, Sogang University Shinsu-Dong, Mapo-Ku, Seoul 121-742, Korea
[2] Korea Simulation Technology Incorporated, B-1303, Koron Lakepolice 2-Cha Janghang-Dong, Ilsan-Ku Koyang-Si, Kyunggi-Do 411-904, Korea

E-mail: bs_ko@naver.com

Received 16 March 2005
Published 17 October 2005
Online at stacks.iop.org/SMS/14/1343

Abstract
This paper deals with the static and dynamic electromechanical responses of piezoelectric layered structures (multimorphs). Based on the Bernoulli–Euler plate model including the dynamics of piezoelectric, electrode and substrate layers, we obtain the natural frequencies, maximum displacement and resultant force of a symmetric cantilevered multimorph. The proposed theoretical model is verified by experiments using a 20-layered PZT (plumbum–zirconate–titanate) multimorph, and it is compared to the conventional bimorph model. Experimental results agree with the analytical predictions on the natural frequencies and vertical displacement. With the analytical solution for multimorph, we investigate the effects of the layer number and the layer thickness on natural frequency, maximum deflection and output force. It is found that there exists an optimum number of piezoelectric layers to maximize the transverse deflection. There also exists a specific value of the thickness ratio between piezoelectric and structure layers to maximize both the tip deflection and force.

1. Introduction

Recently, piezoelectric actuators integrated with structure, which are usually called smart structures or intelligent structures, have often played important roles as actuators in micro-electromechanical systems [1, 2]. These structures, referred to as bimorphs/multimorphs, consist of thin layers of piezoelectric, electrode and elastic materials. The multimorph device operates in a bending mode resulting from the applied electrical loading. The multimorph piezoelectric actuator has several advantages including fast response time and a great resultant force. The many applications have included a printer head [3], an X–Y stage [4], swing CCD mechanisms [5], electro-acoustic transducers, medical devices, microrobots, microscopic cantilevers and micromechanical flying insects [6]. In some cases, high natural frequencies and high displacement/voltage sensitivity are necessary for successful application in controlling the servo mechanism with smart structures [7].

[3] Author to whom any correspondence should be addressed.

Piezoelectric material was first used to measure the vibration of a mechanical system [8, 9]. In addition to the measurement of vibration using the piezoelectric sensor, the piezoelectric actuator is well suited for the control of vibration modes, as it is space efficient, lightweight and requires no external supports [10–12].

Numerous studies have been performed in the linear analysis of a smart structure. Yao *et al* [13] studied a multimorph fabricated by a multiple screen-printing process. They investigated vibration in the transverse (width) direction instead of the longitudinal direction to cause synchronistic deformation of all layers. Yao *et al* [14] investigated the dynamic behavior of multilayered piezoelectric diaphragms that simplified as laminated plates. Rogacheva *et al* [15] studied the dynamic characteristics of a bimorph actuator by electroelasticity theory and experiments. Devoe and Pisano [16] investigated the piezoelectric beam model that described the deflection of a generic multiplayer piezoelectric multimorph. Weinberg [17] proposed a simple close form solution to derive simple working equations for the bending of piezoelectric multimorph using Euler–Bernoulli beam

theory without inverting matrices. Krommer [18] developed the constitutive equations of multimorph by assuming two-dimensional kinematics of the structure. In addition to the theory of elasticity, Ha and Kim [19] investigated the dynamic behavior of piezoelectric actuators by using the impedance and admittance method. And Tamor and Kosa [20] extended the Weinberg analysis to materials with arbitrary electromechanical coupling coefficients by accounting for the variation of electric field in the beam layers.

There have also been numerous studies of the optimization of unimorph, bimorph and multimorph to maximize the tip stroke or vertical displacement using the thickness ratio between substrate and PZT layers. Li *et al* [21] investigated the effect of the thickness ratio to the tip stroke for unimorph only. They showed that there exists an optimal thickness ratio for the simply supported unimorph beam. Ha and Kim [19] showed that there exists an optimal thickness ratio of the middle structure (or shim layer) thickness to the total thickness. The past research works have concentrated on finding the optimal thickness ratio to maximize the tip stroke. There is little work to find the optimum number of layers to maximize the stroke.

The motivation of this work is to find the optimal number and thickness ratio of piezoelectric and structure layers consisting of multimorph for maximizing the tip deflection. To find the optimal number of layers, the authors derive a multimorph model using small piezoelectricity approximation proposed by several authors [15–18, 20] through the elasticity theory and forced harmonic motion analysis. A theoretical model, including the dynamics of multimorph, is derived and it is analytically solved to predict the natural frequency and maximum displacement. The experimental results using PZT layers agree with the analytical predictions. It is discovered that there exists an optimal number of piezoelectric layers to maximize the tip deflection.

2. Theory and modeling of the multimorph

2.1. Constitutive equations of piezoelectric material

The constitutive equations for piezoelectric material can be expressed in terms of the piezoelectric constants which couple the mechanical strain, stress, electric field, and electric displacement based on the IEEE standard on piezoelectricity [22]:

$$\sigma_{ij} = c^E_{ijkl}\varepsilon_{kl} - e_{kij}\mathbf{E}_k \tag{1}$$

$$D_i = e_{ikl}\varepsilon_{kl} + \gamma^\varepsilon_{ik}\mathbf{E}_k \tag{2}$$

where σ_{ij} is the stress tensor, ε_{kl} is the strain tensor, $\mathbf{E}_k$ is the electric field, D_i is the electric displacement (or electric flux density, the charge distributed uniformly over a surface), and c^E_{ijkl}, e_{kij}, and γ^ε_{ik} indicate the stiffness matrix, the piezoelectric stress/charge constant matrix, and the piezoelectric permittivity constant of a piezoelectric material.

Since the stress and strain matrices σ_{ij} and ε_{kl} are symmetric, the matrix notation can be replaced by the vector notation σ_p and ε_q, such that the ij and kl subscripts 11, 22, 33, 12, 13 and 23 correspond to the p and q subscripts 1, 2, 3, 4, 5 and 6. Similarly, the stiffness matrix c^E_{ijkl} and the piezoelectric stress/charge constant matrix e_{kij} can be expressed in the reduced-order matrix notation c^E_{pq} and e_{kp}

$$\sigma_p = c^E_{pq}\varepsilon_q - e_{kp}\mathbf{E}_k \tag{3}$$

$$D_i = e_{iq}\varepsilon_q + \gamma^\varepsilon_{ik}\mathbf{E}_k. \tag{4}$$

The subscript in σ_p and ε_p denotes the normal stress and strain for $p = 1, 2, 3$ and the shear stress and strain for $p = 4, 5, 6$. The piezoelectric stress/charge matrix of the piezoelectric material e_{pq} can be expressed as $e_{pq} = c^E_{qs}d_{ps}$, where d_{ps} represents the piezoelectric strain/charge matrix of the piezoelectric material and is defined as the ratio of the induced strain to the applied field in a stress-free state. For linear, isotropic materials under plane stress, the governing equations become

$$\begin{pmatrix}\sigma_1\\ \sigma_2\\ \sigma_3\end{pmatrix} = [C]\begin{pmatrix}\varepsilon_1\\ \varepsilon_2\\ \varepsilon_3\end{pmatrix} - [C]\begin{pmatrix}d_{31}\mathbf{E}_3\\ d_{31}\mathbf{E}_3\\ 0\end{pmatrix} \tag{5}$$

$$D_3 = \gamma_3\mathbf{E}_3 + d_{31}\mathbf{E}_3 + d_{32}\mathbf{E}_3. \tag{6}$$

2.2. Static analysis of the multimorph

Multimorph piezoelectric actuators are used in cases where large displacements and low applied voltage are needed. However, the multimorph shows a small resultant force and low natural frequency [1]. When a PZT actuator consists of multimorph layers, it can enlarge both the generative force and the resonance frequency, even though applied voltage and manufacturing cost are increased. In general, design variables associated with the multimorph should be properly selected for an optimal performance index [23]. Thus, the authors consider the theoretical modeling and analysis for the development of the multimorph.

A multimorph is bonded to the top and bottom surfaces of the structures and is driven by voltages of the opposite polarity. Therefore, when one is expanded, the other is contracted. As shown in figure 1, the electrode and substrate layers exist between two adjacent PZT layers. Usually a multimorph has a symmetrical structure in the x-direction. Suppose that the total thickness of the PZT actuator is small enough for a slender plate analysis where only the strain ($\varepsilon_{\mathrm{PZT}}$) in the x-direction exists. The following assumptions are made:

(a) the plate thickness is much less than the radius of a curvature induced by the electrical loading,
(b) the cross section of the layers is constant along the length of the plate,
(c) the xz-plane is the plane of symmetry,
(d) the xy-plane is the neutral surface,
(e) plane sections remain as the same plane,
(f) equilibrium requires that the resultant of the stress distribution over the cross section of the plate should equal the bending moment.

Also, assume that the stacked plate is perfectly bonded so that linear motion is generated at the interface. Then one can apply the conventional assumptions on stress and strain distributions to this analysis.

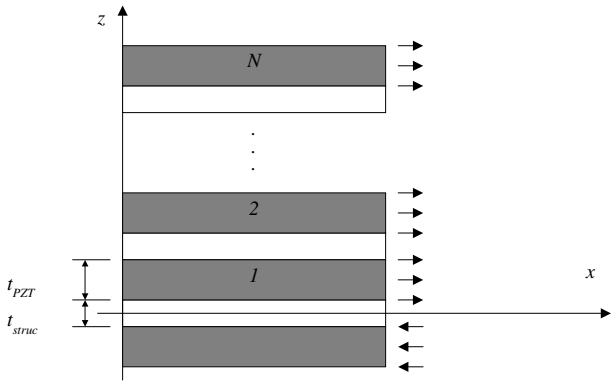

Figure 1. Configuration of a symmetric cantilevered multimorph.

2.3. Analysis of the multimorph

Even if modern piezoelectric actuators are designed to maximize the transfer of energy and thus tend to have large electromechanical coupling coefficients [23], the effect of coupling is not very large for symmetric multimorph [20]. Therefore, the effect of electromechanical coupling is neglected. If PZT is stacked to several layers, the conventional analysis of a single PZT actuator model or a bimorph PZT actuator model is not valid because the moment is generated at each PZT layer. The strain distributions can be represented by

$$\varepsilon = \kappa z. \tag{7}$$

The stress distributions in the structure and PZT can be expressed as

$$\begin{aligned} \sigma_{\text{struc}} &= E_{\text{struc}} \kappa z \\ \sigma_{\text{PZT}} &= E_{\text{PZT}} (\kappa z - \varepsilon_{\text{piezo}}) \end{aligned} \tag{8}$$

where κ represents the curvature of the beam, E_{struc} and E_{PZT} are Young's moduli corresponding to the structure and PZT layer, and σ_{struc} and σ_{PZT} denote the stresses along the z-axis for the structure and the PZT layer. $\varepsilon_{\text{piezo}}$ denotes the strain caused by the transverse-piezoelectric-coupling coefficient d_{31} and the electric field applied across the thickness of the layer V/t_{piezo} [24].

In general, the internal moment balance about the neutral axis for a $2N$-tuple PZT actuator can be expressed as

$$M_y = \sum_{k=1}^{N} \int_{A_k} z\sigma \, \mathrm{d}A = 0 \tag{9}$$

when there is no external axial force and bending moment.

Equation (9) can be written in another form as

$$M_y = \sum_{k=1}^{N} \int_{A_k} z\sigma_{\text{struc}} \, \mathrm{d}A + \sum_{k=1}^{N} \int_{A_k} z\sigma_{\text{PZT}} \, \mathrm{d}A = 0. \tag{10}$$

There is one unknown, the curvature κ, to be solved by moment equilibrium. Substituting equation (8) into (11), we can derive the equation related to curvature κ as follows:

$$\begin{aligned} &\sum_{k=1}^{N} \int_{A_k} z^2 \kappa E_{\text{struc}} \, \mathrm{d}A + \sum_{k=1}^{N} \int_{A_k} z^2 \kappa E_{\text{PZT}} \, \mathrm{d}A \\ &= \sum_{k=1}^{N} \int_{A_k} z E_{\text{PZT}} \varepsilon_{\text{piezo}} \, \mathrm{d}A. \end{aligned} \tag{11}$$

$$\begin{aligned} &\kappa \left\{ \sum_{k=1}^{N} \int_{A_k} z^2 E_{\text{struc}} \, \mathrm{d}A + \sum_{k=1}^{N} \int_{A_k} z^2 E_{\text{PZT}} \, \mathrm{d}A \right\} \\ &= \sum_{k=1}^{N} \int_{A_k} z E_{\text{PZT}} \varepsilon_{\text{piezo}} \, \mathrm{d}A. \end{aligned} \tag{12}$$

The following equation can be derived after some mathematical manipulation.

$$\begin{aligned} \kappa &= \frac{\sum_{k=1}^{N} \int_{A_k} z E_{\text{PZT}} \varepsilon_{\text{piezo}} \, \mathrm{d}A}{\left\{ \sum_{k=1}^{N} \int_{A_k} z^2 E_{\text{struc}} \, \mathrm{d}A + \sum_{k=1}^{N} \int_{A_k} z^2 E_{\text{piezo}} \, \mathrm{d}A \right\}} \\ &= \left\{ \sum_{k=1}^{N} \bar{z}_{k,\text{PZT}} E_{\text{PZT}} t_{\text{PZT}} \varepsilon_{\text{piezo}} \right\} \left\{ \sum_{k=1}^{N} E_{\text{PZT}} (I_{\text{PZT}} + t_{\text{PZT}} \bar{z}_{k,\text{PZT}}^2) \right. \\ &\quad \left. + \sum_{k=1}^{N} E_{\text{struc}} (I_{\text{struc}} + t_{\text{struc}} \bar{z}_{k,\text{struc}}^2) \right\}^{-1} \end{aligned} \tag{13}$$

where I_{PZT} and I_{struc} represent the moments of inertia of the PZT layer and structure based on their own neutral axes, and $\bar{z}_{k,\text{PZT}}$ and $\bar{z}_{k,\text{struc}}$ denote the distances from the global neutral surface to their own neutral axes. We define β as the ratio of the structure thickness, t_{struc}, to the combinational thickness, $h = t_{\text{PZT}} + t_{\text{struc}}$, where t_{PZT} is the PZT thickness. Then, $(1-\beta)$ represents the ratio of the PZT thickness to the combinational thickness. Then the numerator in equation (13), bending moment M_E per unit width due to PZT layers, can be expressed as

$$\begin{aligned} M_E &= \sum_{k=1}^{N} \bar{z}_{k,\text{PZT}} E_{\text{PZT}} t_{\text{PZT}} \varepsilon_{\text{piezo}} \\ &= \sum_{k=1}^{N} \left\{ (k-1)h + \left(\frac{1+\beta}{2} \right) h \right\} \\ &\quad \times E_{\text{PZT}} \{(1-\beta)h\} d_{31} \frac{V_{\text{in}}}{\{(1-\beta)h\}} \\ &= h d_{31} E_{\text{PZT}} V_{\text{in}} \sum_{k=1}^{N} \left(k + \frac{\beta - 1}{2} \right). \end{aligned} \tag{14}$$

It is identical to the bending moment due to PZT layers proposed by Tamor and Kosa [20] if $\beta = 0$, $\xi = 0$ and $N = 1$ (two layers). The denominator, total stiffness EI_{total} per unit width, can be written as

$$\begin{aligned} EI_{\text{total}} &= \sum_{k=1}^{N} E_{\text{PZT}} \left(I_{\text{PZT}} + t_{\text{PZT}} \bar{z}_{k,\text{PZT}}^2 \right) \\ &\quad + \sum_{k=1}^{N} E_{\text{struc}} \left(I_{\text{struc}} + t_{\text{struc}} \bar{z}_{k,\text{struc}}^2 \right) \\ &= \sum_{k=1}^{N} E_{\text{PZT}} \left[\frac{(1-\beta)^3 h^3}{12} \right. \\ &\quad \left. + (1-\beta)h \left\{ (k-1)h + \frac{1+\beta}{2} h \right\}^2 \right] \\ &\quad + \sum_{k=1}^{N} E_{\text{struc}} \left[\frac{\beta^3 h^3}{12} + \beta h \left\{ (k-1)h + \frac{\beta}{2} h \right\}^2 \right] \\ &= h^3 \left\{ E_{\text{PZT}} \sum_{k=1}^{N} \left[\frac{(1-\beta)^3}{12} + (1-\beta) \left(k + \frac{\beta - 1}{2} \right)^2 \right] \right. \\ &\quad \left. + E_{\text{struc}} \sum_{k=1}^{N} \left[\frac{\beta^3}{12} + \beta \left(k - 1 + \frac{\beta}{2} \right)^2 \right] \right\}. \end{aligned} \tag{15}$$

Finally, the curvature is

$$\kappa = \left[d_{31} E_{\mathrm{PZT}} V_{\mathrm{in}} \sum_{k=1}^{N} \left(k + \frac{\beta - 1}{2} \right) \right] \times \left[h^2 \left\{ E_{\mathrm{PZT}} \sum_{k=1}^{N} \left[\left(\frac{1-\beta}{12} \right)^3 + (1-\beta) \left(k + \frac{\beta - 1}{2} \right)^2 \right] + E_{\mathrm{struc}} \sum_{k=1}^{N} \left[\frac{\beta^3}{12} + \beta \left(k - 1 + \frac{\beta}{2} \right)^2 \right] \right\} \right]^{-1}. \quad (16)$$

The Euler beam equation was adopted to obtain the maximum transverse deflection along the centerline for a cantilever beam.

$$\delta = \frac{1}{2} \kappa L^2 = \frac{M_E L^2}{2 E I_{\mathrm{total}}} \quad (17)$$

where L is the length of the beam and M_E is the bending moment generated by PZT layers. Using the basic structure formulation, the resultant force to deflect the tip of the beam becomes [25]

$$P = \frac{3 E I_{\mathrm{total}} \delta}{L^3} \quad (18)$$

where $E I_{\mathrm{total}}$ denotes the total stiffness of the multimorph including PZT and structures and is expressed as

$$\begin{aligned} E I_{\mathrm{total}} &= \sum_{k=1}^{N} E_{\mathrm{PZT}} (I_{\mathrm{PZT}} + t_{\mathrm{PZT}} \bar{z}_{k,\mathrm{PZT}}^2) + \sum_{k=1}^{N} E_{\mathrm{struc}} (I_{\mathrm{struc}} + t_{\mathrm{struc}} \bar{z}_{k,\mathrm{struc}}^2) \\ &= h^3 \left\{ E_{\mathrm{PZT}} \sum_{k=1}^{N} \left[\frac{(1-\beta)^3}{12} + (1-\beta) \left(k + \frac{\beta - 1}{2} \right)^2 \right] + E_{\mathrm{struc}} \sum_{k=1}^{N} \left[\frac{\beta^3}{12} + \beta \left(k - 1 + \frac{\beta}{2} \right)^2 \right] \right\}. \end{aligned} \quad (19)$$

If the multimorph is assumed to be the plate model instead of the beam model, the maximum transverse deflection along the centerline should be changed because the plate is subjected to uniform distributed bending moment along its edges, the x- and y-axes. In this case the maximum transverse deflection along the centerline can be expressed as [26]

$$\delta = \tfrac{1}{2} \kappa L^2 (1 - \nu) \quad (20)$$

where ν is the Poisson's ratio under the assumption that the Poisson's ratios of structure and PZT are the same.

If $\beta = 0$, the curvature κ for the beam can be expressed as

$$\kappa = \frac{d_{31} E_{\mathrm{PZT}} V_{\mathrm{in}} \sum_{k=1}^{N} \left(k - \frac{1}{2} \right)}{h^2 \left\{ E_{\mathrm{PZT}} \sum_{k=1}^{N} \left[\left(\frac{1}{12} \right)^3 + \left(k - \frac{1}{2} \right)^2 \right] \right\}}. \quad (21)$$

In particular, when there is a bimorph actuator, $N = 1$,

$$\kappa = \frac{3 d_{31} V_{\mathrm{in}}}{2 h^2} \quad (22)$$

and

$$\delta = \frac{1}{2} \kappa L^2 = \frac{1}{2} \frac{3 d_{31} V_{\mathrm{in}}}{2 h^2} L^2 = \frac{3 d_{31} V_{\mathrm{in}}}{4 h^2} L^2. \quad (23)$$

The above equations are the same as the formula expressed in [27] because h in this formulation is $h_{\mathrm{total}}/2$ in [27].

2.4. Dynamic analysis using the Euler beam

To understand the dynamic properties of the multimorph, a dynamic analysis of the PZT model was carried out. The frequency range under consideration in the vibration control area is much lower in comparison to the thickness and length resonance frequencies of the distributed actuator, which are typically over 20 kHz. Therefore, its effect can also be neglected in the dynamic behavior of a composite structure.

The mathematical modeling of a cantilever beam is considered. The equation of motion for a beam can be represented as follows [24]:

$$E I \frac{\partial^4 w}{\partial x^4} + m' \frac{\partial^2 w}{\partial t^2} = \frac{\partial^2 M_{\mathrm{total}}}{\partial x^2} \quad (24)$$

where M_{total} is a line moment due to control input and m' is mass per unit length of a beam. The bending moment M_{total} is obtained from

$$M_{\mathrm{total}} = \kappa E_{\mathrm{struc}} (I_{\mathrm{struc}})_{\mathrm{total}} \cdot (\langle x - L \rangle^0 - \langle x \rangle^0) \quad (25)$$

where $\langle x \rangle^0$ denotes a unit step function and $(I_{\mathrm{struc}})_{\mathrm{total}}$ represents the total moment of inertia corresponding to the structure. Using equation (13), the bending moment becomes

$$\begin{aligned} M_{\mathrm{total}} &= \frac{\sum_{k=1}^{N} \int_{A_k} z E_{\mathrm{PZT}} \varepsilon_{\mathrm{piezo}} \, \mathrm{d}A \cdot \sum_{k=1}^{N} \int_{A_k} z^2 E_{\mathrm{struc}} \, \mathrm{d}A}{\left\{ \sum_{k=1}^{N} \int_{A_k} z^2 E_{\mathrm{struc}} \, \mathrm{d}A + \sum_{k=1}^{N} \int_{A_k} z^2 E_{\mathrm{PZT}} \, \mathrm{d}A \right\}} \times (\langle x - L \rangle^0 - \langle x \rangle^0) \\ &= \left\{ \left[\sum_{k=1}^{N} \bar{z}_{k,\mathrm{PZT}} E_{\mathrm{PZT}} t_{\mathrm{PZT}} \varepsilon_{\mathrm{piezo}} \cdot \sum_{k=1}^{N} E_{\mathrm{PZT}} (I_{\mathrm{PZT}} + t_{\mathrm{PZT}} \bar{z}_{k,\mathrm{PZT}}^2) \right] \times \left[\sum_{k=1}^{N} E_{\mathrm{PZT}} (I_{\mathrm{PZT}} + t_{\mathrm{PZT}} \bar{z}_{k,\mathrm{PZT}}^2) + \sum_{k=1}^{N} E_{\mathrm{struc}} (I_{\mathrm{struc}} + t_{\mathrm{struc}} \bar{z}_{k,\mathrm{struc}}^2) \right]^{-1} \right\} \cdot (\langle x - L \rangle^0 - \langle x \rangle^0). \end{aligned} \quad (26)$$

Finally, the bending moment can be expressed as

$$\begin{aligned} M_{\mathrm{total}} = \Bigg[& d_{31} E_{\mathrm{PZT}} V_{\mathrm{in}} \sum_{k=1}^{N} \left(k + \frac{\beta - 1}{2} \right) \\ & \times E_{\mathrm{struc}} \sum_{k=1}^{N} \left[\frac{\beta^3}{12} + \beta \left(k - 1 + \frac{\beta}{2} \right)^2 \right] \\ & \times (\langle x - L \rangle^0 - \langle x \rangle^0) \Bigg] \Bigg[\Bigg\{ E_{\mathrm{PZT}} \sum_{k=1}^{N} \Bigg[\left(\frac{1-\beta}{12} \right)^3 \\ & + (1-\beta) \left(k + \frac{\beta - 1}{2} \right)^2 \Bigg] \\ & + E_{\mathrm{struc}} \sum_{k=1}^{N} \left[\frac{\beta^3}{12} + \beta \left(k - 1 + \frac{\beta}{2} \right)^2 \right] \Bigg\} \Bigg]^{-1}. \end{aligned} \quad (27)$$

By oscillating the voltage applied to the actuator, the induced line moment M_{total} will oscillate at the same frequency. Using the modal representation of

$$w_{(x,t)} = \sum_{n=1}^{\infty} \eta_{(t)} \phi_{(x)}, \quad (28)$$

the partial differential equation can be transformed to

$$EI\sum_n \eta_{(t)}\frac{\mathrm{d}^4\phi_n}{\mathrm{d}x^4} + m'\sum_n \phi_n \ddot{\eta}_{(t)} = \frac{\partial^2 M_{\text{total}}}{\partial x^2}. \tag{29}$$

The right-hand side can be represented as follows:

$$\frac{\partial^2 M_{\text{total}}}{\partial x^2} = \bar{C}V_{(t)}(\langle x-L\rangle^{-2} - \langle x\rangle^{-2}) \tag{30}$$

where $\bar{C}$ is a constant, which depends on the properties of the multimorph, expressed as

$$\begin{aligned}\bar{C} = &\left(d_{31}E_{\text{PZT}}\sum_{k=1}^{N}\left(k+\frac{\beta-1}{2}\right)\right.\\ &\times E_{\text{struc}}\sum_{k=1}^{N}\left[\frac{\beta^3}{12}+\beta\left(k-1+\frac{\beta}{2}\right)^2\right]\Bigg)\\ &\times\left(\left\{E_{\text{PZT}}\sum_{k=1}^{N}\left[\left(\frac{1-\beta}{12}\right)^3+(1-\beta)\left(k+\frac{\beta-1}{2}\right)^2\right]\right.\right.\\ &\left.\left.+E_{\text{struc}}\sum_{k=1}^{N}\left[\frac{\beta^3}{12}+\beta\left(k-1+\frac{\beta}{2}\right)^2\right]\right\}\right)^{-1}.\end{aligned} \tag{31}$$

Multiplying by $\phi_m(x)$, integrating over the entire length of the beam and using the orthogonal condition leads to

$$m'\ddot{\eta}_{m(t)} + EI\left(\frac{\lambda_m}{L}\right)^4\eta_{m(t)} = b_m V_{(t)} \tag{32}$$

where $V_{(t)}$ is applied input voltage. The representation of $b_m V_{(t)}$ is defined by

$$\begin{aligned}b_m V_{(t)} &= \int_0^L \phi_m\frac{\partial^2 M_{\text{total}}}{\partial x^2}\,\mathrm{d}x\\ &= \bar{C}V\left(\left.\frac{\mathrm{d}\phi_m}{\mathrm{d}x}\right|_{x=L} - \left.\frac{\mathrm{d}\phi_m}{\mathrm{d}x}\right|_{x=0}\right).\end{aligned} \tag{33}$$

Assuming the harmonic motion and applying the boundary conditions, the associated eigenfunctions can be expressed as

$$\begin{aligned}\phi_n(x) = &(\sin\beta_n L - \sinh\beta_n L)(\sin\beta_n x - \sinh\beta_n x)\\ &+(\cos\beta_n L + \cosh\beta_n L)(\cos\beta_n x - \cosh\beta_n x)\end{aligned} \tag{34}$$

and the fundamental natural frequency becomes

$$\omega_1 = \sqrt{\frac{1.875\,104^4 EI_{\text{total}}}{m'L^4}} \tag{35}$$

where

$$\begin{aligned}EI_{\text{total}} = h^3\left\{E_{\text{PZT}}\sum_{k=1}^{N}\left[\frac{(1-\beta)^3}{12}+(1-\beta)\left(k+\frac{\beta-1}{2}\right)^2\right]\right.\\ \left.+E_{\text{struc}}\sum_{k=1}^{N}\left[\frac{\beta^3}{12}+\beta\left(k-1+\frac{\beta}{2}\right)^2\right]\right\}.\end{aligned}$$

If the multimorph is assumed to be the plate model instead of the beam model, the natural frequencies should also be changed because the plate is subjected to a uniform distributed bending moment along its edges, the x- and y-axes. In this case the first natural frequency can be expressed as

$$\omega_1 = \sqrt{\frac{1.875\,104^4 EI_{\text{total}}}{m'L^4(1-\nu^2)}} \tag{36}$$

where ν is the Poisson's ratio under the assumption that the Poisson's ratios of the structure and PZT are the same.

If $\beta = 0$, the curvature κ for the beam can be expressed as

$$EI_{\text{total}} = h^3 E_{\text{PZT}}\sum_{k=1}^{N}\left[\tfrac{1}{12}+\left(k-\tfrac{1}{2}\right)^2\right]. \tag{37}$$

In particular, when there is one bimorph PZT actuator ($N = 1$),

$$EI_{\text{total}} = \tfrac{1}{3}h^3 E_{\text{PZT}} \tag{38}$$

and

$$\omega_1 = \sqrt{\frac{1.875\,104^4\,\frac{1}{3}h^3 E_{\text{PZT}}}{m'L^4}} = \frac{1.875^2 h}{L^2}\sqrt{\frac{E_{\text{PZT}}}{3\rho_{\text{PZT}}}}. \tag{39}$$

The above equations are the same as the conventional bimorph formula expressed in [27] because h in this formulation is $h_{\text{total}}/2$ in [27].

2.5. *Optimal design of the multimorph*

In this section, the main performance indices such as the maximum stroke, output force, and first natural frequency are optimized using the analytical approach. The total size of the PZT actuator is 16 mm × 6 mm × 0.48 mm. The total number of layers is 20, and each layer thickness is 20 μm. The thickness of each cover layer that is attached to both sides of the multimorph is 40 μm. Titanium is used as the material of the cover layer.

Figures 2(a)–(c) show the profiles of the displacement at the tip position, the first natural frequency, and the resultant force when the total thickness is constant at 0.48 mm and the number of layers is changed from 2 to 20. Here, the total thickness is the summation of PZT, the electrode, and cover layers, which are 400, 40 and 40 μm, respectively. In figures 2(a)–(c), the resultant force, fundamental frequency and displacement increase monotonically with the layer number when the total thickness is kept as 0.48 mm.

Figures 3(a)–(c) represent the variations of the vertical displacement, the first natural frequency, and resultant force when the thickness of each layer is constant at 20 μm and the total thickness increases with increasing layer number. Contrary to the previous case where the total thickness is constant, the vertical displacement is generally decreased for large layer numbers, if each layer has the same thickness. As shown in figure 3(a), the vertical displacement is increased from two to eight layers, and there exists a maximum stroke at a specific layer number. The existence of the optimal layer number to maximize the tip stroke can be inferred from equation (16), where the numerator in the equation is linearly proportional to the layer number while the denominator is proportional to the square of the layer number.

For the eight-layered multimorph that maximizes the tip stroke, the effect of the thickness ratio to the tip stroke is shown in figures 4(a)–(c). The variations of the vertical displacement, the first natural frequency, and resultant force are plotted when the thickness of each layer is constant at 20 μm and the number of the bimorph PZT is eight. In this case, it is found that the tip stroke and the resultant force are maximized when $\beta = 0.275$ based on the results. When the layer number is six ($N = 3$),

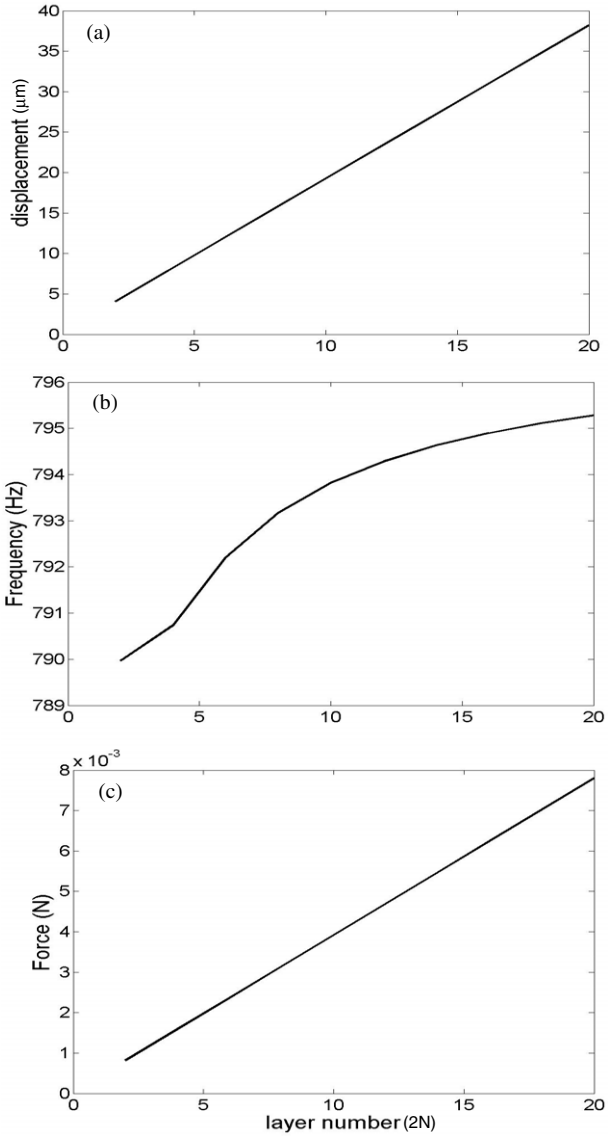

Figure 2. Maximum displacement, fundamental frequency and resultant force with increasing layer number when the total thickness is constant.

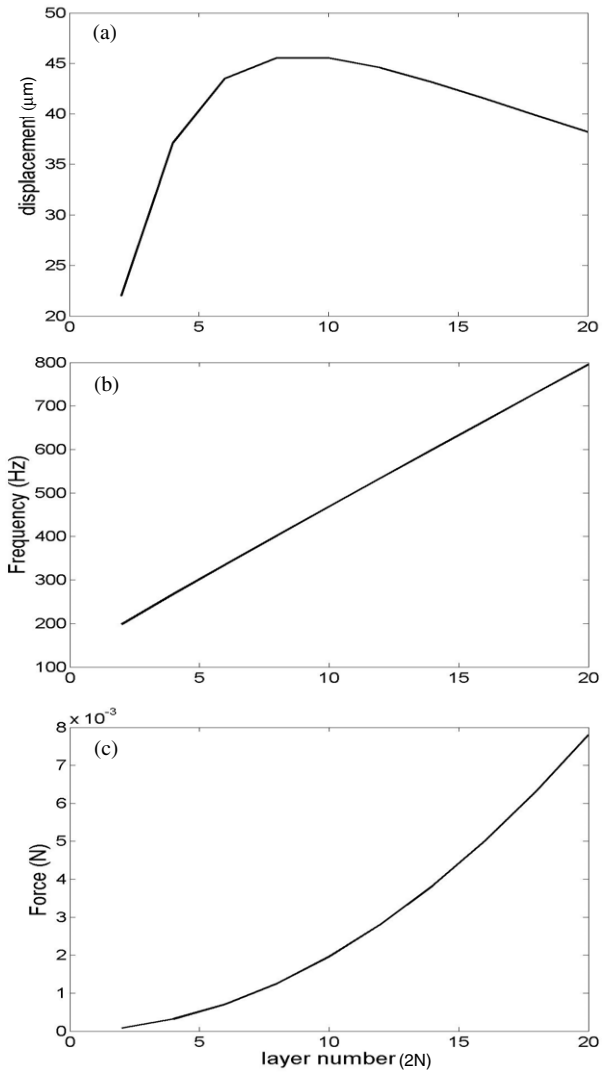

Figure 3. Maximum displacement, fundamental frequency and resultant force with increasing layer number and total thickness when the single layer thickness is constant.

the effect of the thickness ratio on the tip stroke, frequency and force is shown in figures 5(a)–(c). In this case, it is found that the tip stroke and the resultant force are maximized when $\beta = 0.88$ based on the results. This results show that the optimal thickness ratio exists in specific layer numbered multimorph only. In order to find the existence of the optimal thickness ratio at other layer numbers, we draw a three-dimensional plot for layer number, thickness ratio and displacement in figure 6(a). It is found that there exist optimal thickness ratios for maximum displacement only at $N = 3$ and 4. When N is 1 or 2, the displacement monotonically increases with increasing the thickness ratio. However, when the layer number is larger than $N = 4$, the tip stroke decreases with increasing the thickness ratio. Figure 6(b) shows the contour plot of the displacement in the layer number–thickness ratio graph. Local maximum displacements occur only at $\beta = 0.275$ and 0.88.

In contrast to this work, Li *et al* [21] investigated the effect of the thickness ratio to the tip stroke for unimorph only. They showed that there exists an optimal thickness ratio at $\beta = 0.38$ for the simply supported unimorph beam. Ha and Kim [19] showed that there exists an optimal thickness ratio of the middle structure (or shim layer) thickness, $t_{\text{mid\_struc}}$, to the combinational thickness, $h = (t_{\text{PZT}})_{\text{total}} + t_{\text{mid\_struc}}$, where $(t_{\text{PZT}})_{\text{total}}$ is the total thickness of PZT layers. They considered that multimorph does not have any substrate or structure layer except the middle structure or shim layer.

The existence of the maximum displacement can be used for optimal selection of a layer number with a proper resultant force. Actuator designers can determine the layer number and the thickness of PZT by using the above profiles to satisfy an objective like maximum vertical deflection.

3. Experimental results

When a PZT actuator is designed, the performance indices to be optimized are the maximum displacement, the generative force and the mode frequency. In order to verify the validity

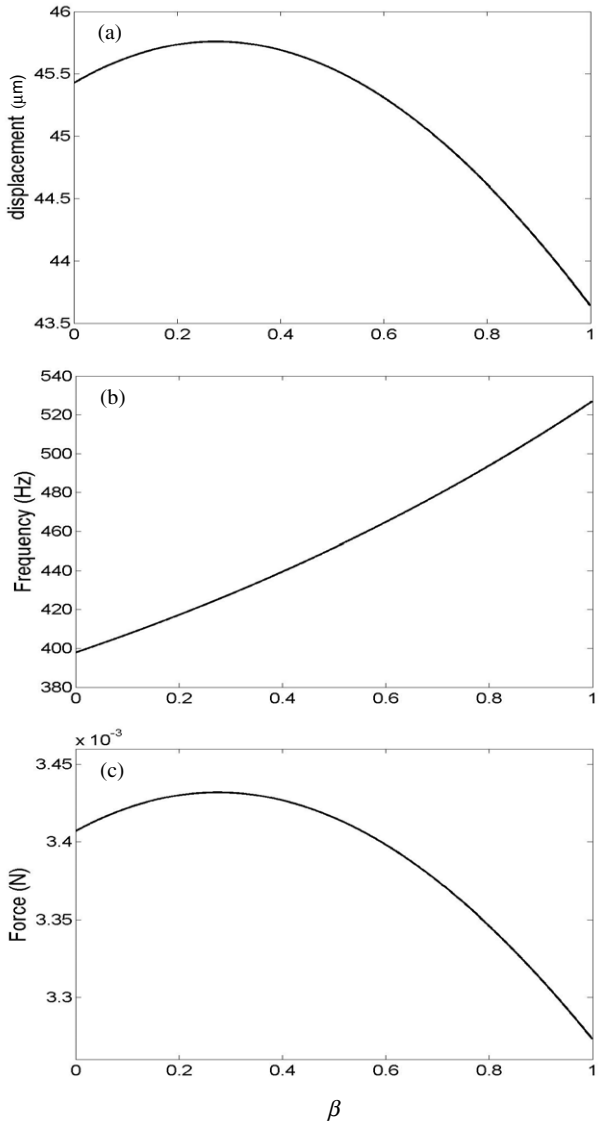

Figure 4. Maximum displacement, fundamental frequency and resultant force as a function of β when the number of layers is eight.

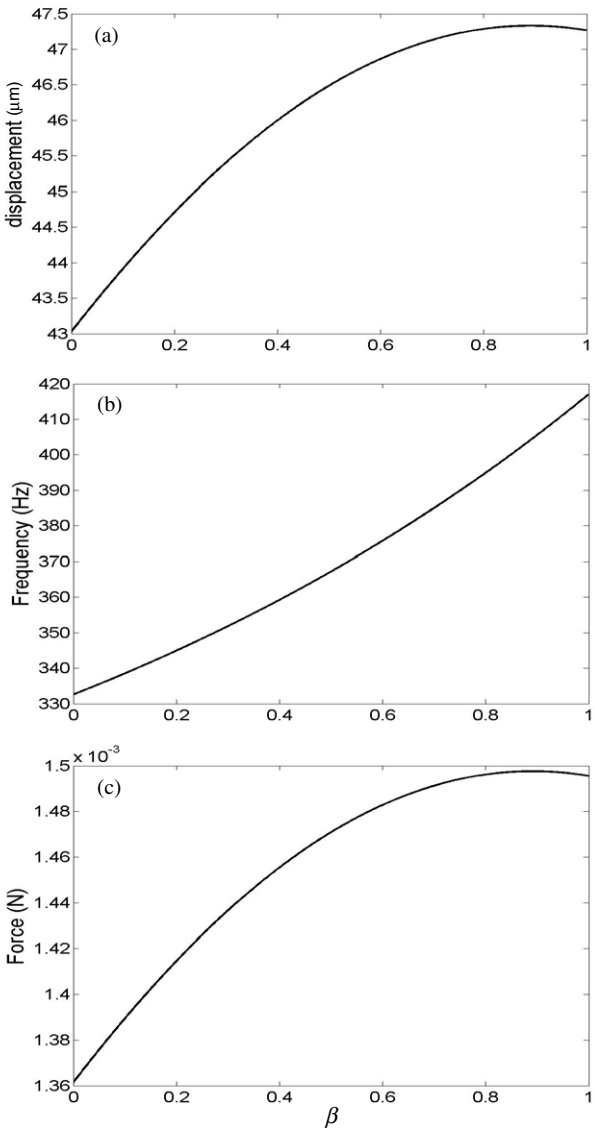

Figure 5. Maximum displacement, fundamental frequency and resultant force as a function of β when the number of layers is six.

of the analytical results on these parameters derived in the above section, experiments were performed with a commercial multimorph.

3.1. Experimental apparatus setup and procedures

Figure 7 shows the schematic diagram of an experimental apparatus setup. The displacement is measured using a MTI-2000 Fotonic sensor with the sensitivity of 0.02 μm mV^{-1}. The MTI-2000 Fotonic sensor is a dual-channel, fiber-optic measurement system that performs non-contact displacement and vibration measurements. In the measurement, sinusoidal waveform electric fields were applied to the actuator. A voltage was applied in a bipolar waveform at 0.05 Hz. The measured data were collected and analyzed by using DSP Siglab and Matlab. In the experiments, a commercial multimorph, manufactured by Morgan Electro Ceramics, was used. The properties of PZT are shown in table 1.

The actuator size is 16 mm $\times$ 6 mm $\times$ 0.48 mm. The material is composed of PbO (66%), ZrO_2 (21%), and TiO_2 (11%). The electrode consists of Ag–Pd. The total number of layers is 20, and each layer thickness is 20 μm. The thickness of each cover layer that is attached to both sides of a multimorph is 40 μm. Titanium is used as the material of the cover layer.

Table 1. Properties of the PZT material.

Property	Values	Unit
Density	7.9×10^3	kg m^{-3}
Dielectric constant	3000	
Coupling factor	0.62	
d_{31} charge constant	-240×10^{-12}	m V^{-1}
Young's modulus	50×10^9	Pa

3.2. Experimental results and discussion

The transverse displacement of a multimorph as a function of the voltage applied across the thickness of the PZT is shown in figure 8. The displacement generally increases

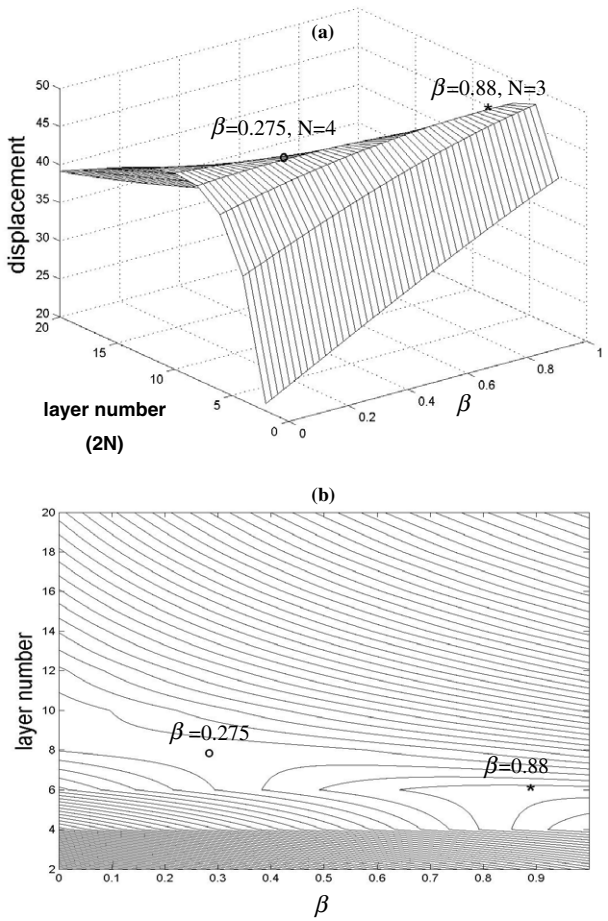

Figure 6. (a) 3D plot of displacement, layer number and thickness ratio, (b) contour line of displacement and existence of the optimal thickness ratio at $N = 3$ and 4.

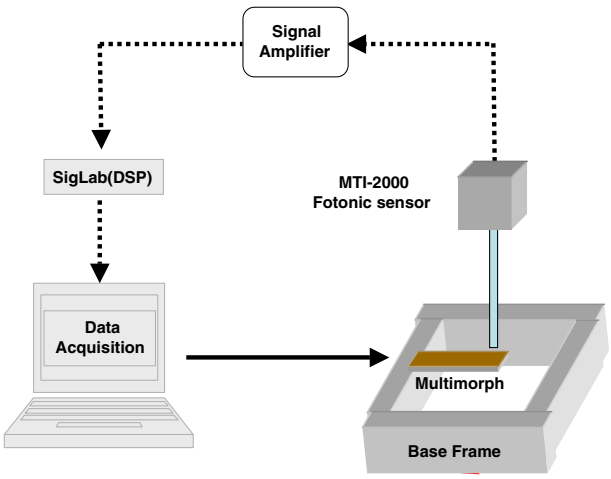

Figure 7. Experimental setup for a cantilevered multimorph. (This figure is in colour only in the electronic version)

with an increasing applied electric field, showing hysteretic motion. The displacement obtained when the applied voltage is decreased from 0 to −10 V is somewhat larger than when

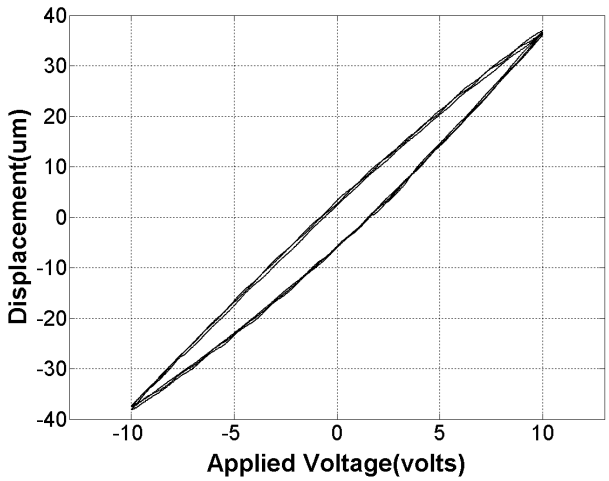

Figure 8. Hysteresis of multimorph.

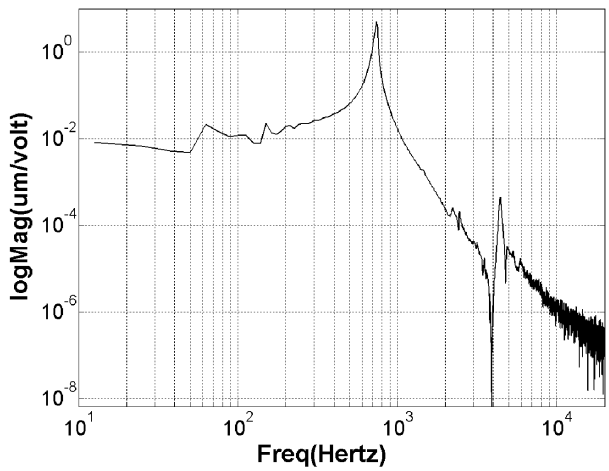

Figure 9. Impulse spectrum graph of multimorph.

the voltage is increased from −10 to 0 V. The hysteretic behavior of the PZT comes from the switching of polarization in PZT when an electric field is increased or decreased. To facilitate switching, an electric field is required to overcome the switching inertia. This is also the reason for the small change of displacement versus the change of applied voltage at low fields (around −10 V) and where fields are reversed (around 10 V). The phenomena in the multimorph are the same as those in the reference by Li *et al* [21]. The maximum displacement is measured as 37 μm.

Figure 9 shows the impulse response plot. The resonance frequencies of the multimorph were measured with a frequency analyzer in the frequency range of 10 Hz–20 kHz. Figure 10 shows the FRF (frequency response function) of the multimorph when the actuator is excited by a banded-white noise from 10 Hz to 20 kHz. The fundamental natural frequency of the PZT actuator is 750 Hz as shown in figures 9 and 10.

The theoretical results by the Bernoulli–Euler plate model and experimental results are summarized in table 2. The theoretical results show a good correlation compared with the experimental data. Because the theoretical predictions agree

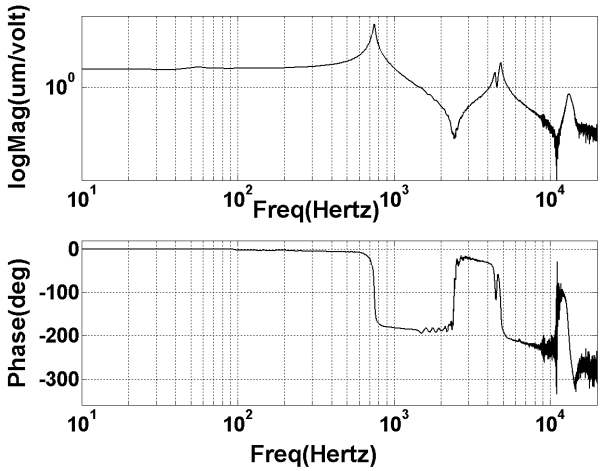

Figure 10. FRF graph of the multimorph.

Table 2. Comparisons of experimental and analytical results of multimorph.

	Theory	Experiment	Experiment (provided by manufacturer)
Displacement (μm)	$\pm$38.20	$\pm$36.96	$\pm$38.54
1st mode (Hz)	795.2	750	750
2nd mode (Hz)	4983.4	4837.5	—
3rd mode (Hz)	13 954	14 544	—

with the experimental results, they can be used as a theoretical model in designing the PZT actuator.

It is useful to make a comparison with a well-known bimorph actuator in validating the multimorph model. The fundamental natural frequency f and maximum deflection δ of the bimorph actuator are expressed as follows [27]:

$$f = \frac{1.875^2 h_{\text{total}}}{4\pi L^2}\sqrt{\frac{E_{\text{PZT}}}{3\rho_{\text{PZT}}}} \tag{40}$$

$$\delta = \frac{3L^2}{h_{\text{total}}^2} d_{31} V_{\text{in}} \tag{41}$$

where V_{in} is the input voltage to each PZT layer. The calculated performance indices of the bimorph and multimorph models are listed in table 3. The dimensional data are assumed to be the same as those of the proposed model. The displacement of the bimorph model is just 10% of the experimental data even if the natural frequency is close to the experimental data. It is found that the multimorph model is superior to the conventional bimorph model for describing multimorph based on the result.

4. Conclusions

The authors propose a theoretical modeling of piezoelectric layered structures (multimorphs). A theoretical model of the multimorph includes the dynamics of several piezoelectric, electrode and substrate layers, and it is analytically solved to predict the natural frequency, the resultant force and the maximum displacement of multimorph. Experimental results

Table 3. Comparison between bimorph and multimorph.

	Conventional bimorph model	Multimorph model (theory)	Multimorph model (experiment)
Displacement (μm) ($V_{\text{in}} = 10$ V)	$\pm$3.84	$\pm$38.20	$\pm$36.96
1st mode (Hz)	790.1	795.2	750
2nd mode (Hz)	4951.4	4983.4	4837.5
3rd mode (Hz)	13 864	13 954	14 544

agree with the analytical predictions on the natural frequencies and transverse deflection. With the proposed analytical model, we obtain the effects of the layer number and the electrode thickness to natural frequency, maximum deflection and output force. It is found that there exists an optimal number and thickness of piezoelectric layers to maximize the bending deflection. Multimorph is compared with a conventional bimorph, showing a larger displacement than bimorph.

Acknowledgment

This work was supported by Grant No R11-1997-042-11001-0 of the Korean Science and Engineering Foundation.

References

[1] Srinivasan V 2001 *Smart Structures* (New York: Cambridge University Press)
[2] Muralt P 2000 Ferroelectric thin films for micro-sensors and actuators: a review *J. Micromech. Microeng.* **10** 136–46
[3] Kitahara T 1995 Ink jet head with multiplayer piezoelectric actuator *Proc. IS&T's 11th Int. Congr. on Advances in Non-Impact Printing Technology (Hilton Head, SC)* pp 346–9
[4] Mori K, Kumagae T and Hirai H 1989 Ultrasonic linear motor for a high precision X–Y stage *Proc. IEEE Ultrason. Symp.* **1** 657–60
[5] Li P and Wen Y 1994 Image resolution improvement by swing CCD array imager in two dimensions and its signal processing *Proc. SPIE* **2308** 915–20 (part 2)
[6] Fearing R, Chiang K, Dickinson M, Pick D, Sitti M and Yan J 2000 Wing transmission mechanism for a micromechanical flying insect *Proc. IEEE Int. Conf. on Robotics and Automation (San Francisco, CA)* pp 1509–16
[7] Pokines B J and Garcia E 1998 A smart material microamplification mechanism fabricated using LIGA *Smart Mater. Struct.* **7** 105–12
[8] Lee C K and Moon F C 1990 Modal sensors/actuators *Trans. ASME J. Appl. Mech.* **57** 434–41
[9] Lee C K, Chiang W W and O'Sullivan T C 1991 Piezoelectric modal sensor/actuator pairs for critical active damping vibration control *J. Acoust. Soc. Am.* **90** 374–84
[10] Bailey T and Hubbard J E 1985 Distributed piezoelectric-polymer active vibration control of a cantilever beam *J. Guid. Control* **8** 605–11
[11] Crawley E F and de Luis J 1987 Use of piezoelectric actuators as elements of intelligent structures *AIAA J.* **25** 1373–85
[12] Ko B and Tongue B H 1995 Acoustic control using self-sensing actuator *J. Sound Vib.* **187** 145–65
[13] Yao K, Zhu W, Uchino K, Zhang Z and Lim L C 1999 Design and fabrication of a high performance multilayer piezoelectric actuator with bending deformation *IEEE Trans. Ultrason. Ferroelectr. Freq. Control* **46** 1020–7
[14] Yao L, Lu L, Wang Z, Zhu W and Dai Y 2003 Exact solution of multilayered piezoelectric diaphragms *IEEE Trans. Ultrason. Ferroelectr. Freq. Control* **50** 1262–71

[15] Rogacheva N N, Chou C C and Chang S H 1998 Electromechanical analysis of a symmetric piezoelectric/elastic laminate structure: theory and experiment *IEEE Trans. Ultrason. Ferroelectr. Freq. Control* **45** 285–94
[16] De Voe D L and Pisano A P 1997 Modeling and optimal design of piezoelectric cantilever microactuators *J. Microelectr. Syst.* **6** 266–70
[17] Weinberg M S 1999 Working equations for piezoelectric actuators and sensors *J. Microelectr. Syst.* **8** 529–33
[18] Krommer M 2001 On the correction of the Bernoulli–Euler beam theory for smart piezoelectric beams *Smart Mater. Struct.* **10** 668–80
[19] Ha S K and Kim Y H 2002 Analysis of a piezoelectric multimorph in extensional and flexural motions *J. Sound Vib.* **253** 1001–14
[20] Tadmor E B and K'osa G 2003 Electromechanical coupling correction for piezoelectric layered beams *J. Microelectromech. Syst.* **12** 899–906
[21] Li X, Shih W Y, Aksay I A and Shih W-H 1999 Electromechanical behavior of PZT-brass unimorphs *J. Am. Ceram. Soc.* **82** 1733–40
[22] *IEEE Standard on Piezoelectricity* 1988 (New York: IEEE) (ANSI/IEEE Std. 176-1987)
[23] Park S E and Shrout T R 1997 Ultrahigh strain and piezoelectric behavior in relaxor based ferroelectric single crystals *J. Appl. Phys.* **82** 1804–11
[24] Ko B, Tongue B H and Packard A 1994 Optimal location of distributed sensor/actuator *Shock Vib.* **1** 357–74
[25] Timoshenko S P and Gere J M 1972 *Mechanics of Material* (New York: Van Nostrand-Reinhold)
[26] Ugural A C 1981 *Stresses in Plates and Shells* (New York: McGraw-Hill)
[27] Smits J G, Dalke S L and Cooney T K 1991 The constituent equations of piezoelectric bimorphs *Sensors Actuators* **28** 41–61